Heliyon 9 (2023) e21955

Contents lists available at ScienceDirect

Heliyon

journal homepage: www.cell.com/heliyon

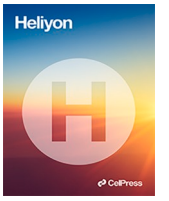

The extract from *Portulaca oleracea* L. rehabilitates skin photoaging via adjusting miR-138-5p/Sirt1-mediated inflammation and oxidative stress

Liping Qu [a,b,c,*], Feifei Wang [a,b,c], Xiao Ma [b,c]

[a] *Innovation Materials Research and Development Center, Botanee Research Institute, Shanghai Jiyan Bio-Pharmaceutical Development Co., Ltd., Shanghai 201702, China*
[b] *Yunnan Characteristic Plant Extraction Laboratory, Yunnan Yunke Characteristic Plant Extraction Laboratory Co., Ltd., Kunming 650106, China*
[c] *Yunnan Botanee Bio-technology Group Co., Ltd., Kunming 650106, China*

ARTICLE INFO

Keywords:
inflammation
Skin photoaging
Purslane extract
miR-138-5p/sirt1 signal

ABSTRACT

Photoaging is the main form of external skin aging, and ultraviolet radiation is the main cause. Long-term ultraviolet radiation can cause oxidative stress, inflammation, immune responses, and skin cell apoptosis. Therefore, it is necessary to explore active products from plants to treat skin photoaging. C57BL/6J mice were randomly divided into control, model, and purslane (*Portulaca oleracea* L.) extract-treated groups (150, 300, and 600 mg/kg). Ultraviolet (UV) radiation induces skin photoaging. Histopathological changes in the skin were observed by hematoxylin and eosin (H&E), Masson's trichrome, and toluidine staining. Levels of hydroxyproline (HYP), hyaluronic acid (HA), collagen I (COL1), catalase (CAT), malondialdehyde (MDA), and total superoxide dismutase (T-SOD) were measured. UVB-induced BJ and HaCaT cells were used to evaluate the effects of the crude extract. The effects of the purslane extract on miR-138-5p/Sirt1 signaling were then tested. The results showed that the purslane extract significantly increased cell viability in UVB-induced cells and decreased oxidative damage and inflammation. In addition, the extract affected the miR-138-5p levels *in vivo* and *in vitro,* and increased the levels of the target gene Sirt1. In UVB-induced cells, purslane extract significantly altered the expression levels of genes or proteins associated with miR-138-5p/Sirt1 signaling. Inflammation and oxidative damage were significantly enhanced when miR-138-5p was overexpressed, and the expression levels of the genes and proteins were reversed by the extract. Co-transfection with the miR-138-5p inhibitor and si-Sirt1 showed the same effects as the extract on the signal. Similar results have been observed in mice. In summary, purslane extract showed potent protective effects against skin photoaging by regulating the miR-138-5p/Sirt1 axis and should be used as a natural product for skin care.

1. Introduction

The skin is the largest organ that protects the body from external damage. With improvements in people's lives, attention paid to

* Corresponding author. Yunnan Botanee Bio-technology Group Co., Ltd., Chuangye Building, 53 Keyi Road, High-tech Zone, Kunming 650106, China.
E-mail address: quliping@winona.cn (L. Qu).

https://doi.org/10.1016/j.heliyon.2023.e21955
Received 18 July 2023; Received in revised form 18 October 2023; Accepted 1 November 2023
Available online 7 November 2023

skin aging is gradually increasing. Some factors including the environment, reactive oxygen species (ROS), telomere shortening, and hormonal changes can cause skin damage [1]. The primary condition may be caused by UV radiation, which induces skin photoaging [2]. After receiving excessive ultraviolet radiation, the cells in the skin tissue can produce oxidative stress and increase ROS levels, destroying the integrity of the cell membrane and antioxidant system and causing inflammation and apoptosis. At the same time, excessive ultraviolet radiation can degrade skin collagen, hyaluronic acid, and elastin, resulting in reduced skin elasticity, roughness, and wrinkles [3,4]. Therefore, the development of effective methods to combat skin damage is extremely important.

Inflammatory response is one of the hallmarks of premature skin aging [5]. Ultraviolet radiation can produce a variety of inflammatory factors, inducing changes and damage to the skin tissue. UV-induced skin photoaging can activate nuclear factor kappa B (NF-κB), which plays a key role in inflammation cascade [6]. Organ damage can also stimulate the production of tumor necrosis factor alpha (TNF-α), interleukin-1alpha (IL-1α), and cycloxygenase-2 (COX-2) [7]. Studies have shown that IL-6 is closely associated with cell growth and skin [8]. Inflammation is often accompanied by ROS accumulation [9]. ROS play an important role in the progression of inflammatory disorders [10]. ROS also play a crucial role in the photoaging process as they can directly damage DNA, resulting in protein inactivation and skin aging [11]. Thus, the regulation of inflammation and ROS is an important method for improving skin photoaging.

MiRNAs are small non-coding RNAs involved in post-transcriptional gene regulation that inhibit translation and destabilize mRNAs to regulate their targets [12]. miRNAs can degrade or hinder the translation of target genes and regulate their expression after transcription [13]. Several studies have shown that miRNAs play critical roles in skin damage. It has been reported that miR-138-5p induces cell invasion by targeting Trp53 expression in murine melanoma cells [14], which inhibits the survival of human melanoma cells [15] and regulates the proliferation and apoptosis of fibroblasts in scar tissues [16]. It has also been reported that miR-138-5p affects hypoxia/reperfusion-induced heart injury [17], pancreatic cancer [18], and other diseases by targeting the silent information regulator Sirtuin 1 (SIRT1), a post-translational regulator with various biological effects [19]. SIRT1 can regulate inflammation by regulating NF-κB signaling [20] which could be an essential drug target against skin aging [21]. However, there are no reports on the role of the miR-138-5p/Sirt1 axis in skin damage.

Recently, many plants, including *Zizania latifolia* [22] and *Cistus* [23], have been used to treat skin photoaging. *Portulaca oleracea* L. (purslane) belongs to the *Portulacaceae* family [24] and is widely distributed in tropical and subtropical areas in the world [25]. In Chinese folklore, purslane is described as a "vegetable for prolonging life," and confirmed as an ancient herbal remedy [26]. It has been reported that purslane extract protects mice from acute liver injury and regulates skin barrier function in acute eczema model rats [27]. In UVB-induced lung injury in rats, purslane suppressed lung inflammation by reduction of IL-β, IL-6, TNF-α, TGF-β, and IL-10 levels [28]. However, the effect of purslane extract on skin photoaging has not been reported.

In the present study, UV-induced skin injury in mice and UVB-induced BJ and HaCaT cells were used to evaluate the pharmacological effects of the extract and the possible mechanisms of action of miR-138-5p/Sirt1 were tested.

2. Materials and methods

2.1. Chemicals and materials

Hydroxyproline (HYP), hyaluronic acid (HA), and collagen type I (CoL I) detection kits were purchased from Nanjing Jiancheng Institute of Biotechnology (Nanjing, China). Philips PL-S 9W/01 was purchased from Philips (Netherlands). An immunohistochemistry kit was purchased from ZSGB-Bio (Beijing, China). RIPA buffer, PMSF, and the BCA Protein Assay Kit were purchased from Beyotime Biotechnology (Jiangsu, China). TransDetect® Double-Luciferase Reporter Assay Kit, TransZolTM, TransScript® All-in-One First-Strand cDNA Synthesis SuperMix for RT-PCR (One-Step gDNA Removal) and TransStart® Top Green RT-PCR SuperMix were obtained from Beijing TransGen Biotech Co., Ltd. (Beijing, China). miR-138-5p mimic, inhibitor, and their negative control (NC) oligos, wild-type Sirt1 (Sirt1-WT), 3′UTR-mutated Sirt1 (Sirt1-MUT) luciferase, Sirt1 siRNA, lipofectamin2000, and FISH fluorescent probe were all constructed by GenePharma Company (Suzhou, China). The miRNA extraction, first-strand cDNA synthesis, and quantitative PCR kits were provided by Sangon Biological Engineering Technology & Services Co., Ltd. (Shanghai, China).

2.2. Preparation of the extract

The purslane extract was obtained from the aboveground part of the purslane plant. Professor Haiyang Liu identified purslane collected in Kunming, Yunnan Province, China in May 2020 (No. 20200518 from the Kunming Institute of Botany, Kunming, China). A purslane voucher specimen (No. 20200518) was deposited in the herbarium of Shanghai Jiyan Bio-Pharmaceutical Development Co. Ltd., Shanghai, China. For the study, 100.0 g of purslane was ground and placed in a 2 L flask with 1000 g of 20 % ethanol reflux extraction for 60 min. After centrifugation, type 767 activated carbon (5.0 g) was added to the supernatant and stirred for 30 min. The total extract was collected and dried to obtain 3.24 g solid powder.

2.3. Analysis of bioactive compounds of purslane extract

The main bioactive compounds in the purslane extract have been confirmed in a previous study [29]. In brief, the contents of organic acid and polysaccharide in the extract were 20%–30 % and 25%–35 %, respectively. The extract was thinned to 4.71 mg/mL and examined using high-performance liquid chromatography [30]. The adenosine content of the extract was 1.46 mg/g.

2.4. Animals

Male C57BL/6J mice (8–9 weeks weight 20 ± 2 g) were obtained from Experimental Animal Center at Dalian Medical University, Dalian, China (SCXK (Liao) 2013-0003). The study was approved by Dalian Medical University ethics committee (approval no. AEE21009). During the study, the mice were kept in groups of 8–10 per cage on a 12-h light/dark cycle in a temperature-controlled (25 ± 2 °C) room with 55–65 % humidity at a special pathogen-free level. They had unlimited access to food and water. The tests were conducted by researchers blinded to the group assignments of each animal. Animal studies were performed in accordance with ARRIVE guidelines [31].

2.5. Animal experimental design

After one week of adaptation, the mice were randomly divided into the following groups: control, model (UV radiation), low dose treatment (UV radiation + 150 mg/kg purslane extract), medium dose treatment (UV radiation + 300 mg/kg purslane extract), high dose treatment (UV radiation + 600 mg/kg purslane extract), and positive treatment (UV radiation + 100 mg/kg Vitamin E); 8 mice were allocated to each group [32]. A UV-induced skin injury model was established using a UV light box. The self-made ultraviolet irradiation box was equipped with six UVA tubes (15 W each, wavelength range 320–400 nm) and three UVB tubes (40 W each, wavelength range 290–320 nm) with an irradiation height of 30 cm. Two days before the experiment, the mice were depilated, forming an exposure area of approximately 4 cm × 3 cm; the fluff on the back of the mice was shaved off with a baby hair clippers and then depilated again with a depilatory cream. The mice in the model, purslane treatment, and positive treatment groups were established as light damage models using ultraviolet irradiation. The modeling conditions were as follows: UVA irradiation intensity 160 μW/cm^2, UVB irradiation intensity 680 μW/cm^2, irradiation time 8 weeks, 3 times/week, 20 min per irradiation in the first week, 40 min per irradiation in the second week, 60 min per irradiation in the third week, and 80 min per irradiation in the fourth to eighth weeks. To prepare the purslane extract gel (VE gel), we dissolved 2 g of carbomer 940 powder in 100 mL water and left it at 4 °C overnight to obtain 2 % carbomer. The next day, an appropriate amount of purslane extract (VE) was dissolved in 10 mL of water, and 30 g of 2 % carbomer was added. The final concentrations of the purslane extract gel were 15 mg/mL, 30 mg/mL and 60 mg/mL for the low-, medium-, and high-dose groups, respectively. The final concentration of VE gel was 10 mg/mL. Triethanolamine was used to adjust the pH until the gel became transparent. Before UV irradiation, 0.2 mL of purslane extract (VE) gel was applied to the shaved area of the mice for 0.5 h, three times a week, for eight weeks [33,34].

2.6. Biochemical analysis

The contents of hydroxyproline (HYP), hyaluronic acid (HA), collagen I (COL1), catalase (CAT), malondialdehyde (MDA), and total superoxide dismutase (T-SOD) were measured using kits.

2.7. Histopathologic examination

Skin tissue fixed with 4 % paraformaldehyde was embedded in paraffin, cut into 5-μm slices, and stained with hematoxylin-eosin, Masson's trichrome, and toluidine blue. Staining was observed, and images were captured using a Nikon TE2000U microscope (Tokyo, Japan).

2.8. Cell culture and model establishment

BJ and HaCaT cells were purchased from Wuhan Procell Life Science & Technology Co., Ltd. (Wuhan, China) and grown in DMEM supplemented with 10 % fetal bovine serum. Cells were seeded in 96-well plates at a density of 1 × 10^6 cells/mL. After washing 2–3 times with PBS buffer, 100 μL PBS buffer was added to cover the cells, which were then placed under a UVB light source for irradiation. In our pre-experiment, we examined the effects of different light intensities (10, 20, 30, 40, 50, 60, 70, 80 mJ/cm^2) on cell toxicity, and the results showed that the tested light intensities all produced cytotoxicity. Based on the cell vitality under different light intensities and the report [35], 30 mJ/cm^2 was set as the intensity for UVB model *in vitro*. After irradiation, the waste liquid was discarded and the cells were cultured under standard conditions for 24 h. Then, 100 μL of incomplete medium containing 10 % MTT (10.0 mg/mL) was added. After shaking for 10 min, absorbance was measured at 490 nm using a microplate analyzer (Multifunctional microplate reader, Thermo, USA).

2.9. Cytotoxicity and protective effect of purslane extract

The cells were seeded into 96-well plates at a concentration of 1 × 10^6 cells/mL (100 μL). Different concentrations of purslane extract (75, 150, 300, 600, 1200, 2400, and 4800 ng/mL) were used at 6, 12, and 24 h. To determine the effect of the extract on the viability of cells induced by UVB, the cells at a concentration of 1 × 10^6 cells/mL were seeded in 96-well plates for 24 h. Different concentrations of the purslane extract (150, 300, and 600 ng/mL) were used for 12 h, followed by UVB. MTT assay was used to detect cell viability.

Table 1
Sequences of RNA primers used in the real-time PCR assay.

Genes	Forward primer (5′-3′)	Reverse primer (5′-3′)
GAPDH	GCCACCCAGAAGACTGTGGAT	GGAAGGCCATGCCAGTGA
U6	CGCTTCGGCAGCACATATACTA	GGAACGCTTCACGAATTTGC
miR-138-5p	GGGAGCTGGTGTTGTGAATCAG	CCAGTGCAGGGTCCGAGGT
Sirt1	TTAAGGCTGTTGGTTCCAGTACTG	CCGTGGAATATGTAACGATTTGG
TNF-α	ACAAGGCTGCCCCGACTAC	TGGGCTCATACCAGGGTTTG
IL-1	CTTTCCCGTGGACCTTCCA	CTCGGAGCCTGTAGTGCAGTT
IL-6	ACCACTCCCAACAGACCTGTCT	CAGATTGTTTTCTGCAAGTGCAT
ICAM-1	CATGGGAATGTCACCAGGAAT	CCTGATCTTTCTCTGGCGGTTA
NQO1	AGCCCTGATTGTACTGGCCC	CCGTTGTCGTACATGGCAGC
GCLM	GAGTTCCCAAATCAGCCCCGA	TGCAACTCCAAGGACGGAGC
GCLC	GCAGCTTTGGGTCGCAAGT	TGGTCTCCAGAGGGTCGGAT

2.10. ROS assay

Cells were seeded in a 24-well plate at a concentration of 1×10^5 cells/mL. After 24 h of culture, 10 μm/mL of DCFH-DA was added and then the cells were incubated for 20 min at 37 °C. Finally, fields were randomly selected using an inverted fluorescence microscope (TE2000U; Nikon, Tokyo, Japan).

2.11. FISH assay

A fluorescent probe was designed based on the miR-138-5p sequence. Cells (5×10^3 cells/mL) were seeded. After 24 h of culture, fluorescent probes, negative controls, and positive controls were introduced into the cells and cell localization was detected using a confocal laser imaging system after transfection (TCS SP5II, Leica, Germany).

2.12. Immunofluorescence assay

The cells were seeded in a 12-well plate. After 24 h of culture, the cells were treated with different concentrations of the purslane extract for 12 h. They were then irradiated with UVB. The samples were fixed with 4 % formaldehyde, blocked with 2 % BSA followed by adding primary antibody Sirt1 (1:50 dilution) and incubated overnight at 4 °C. On the next day, the cells were treated with fluorescein-labeled secondary antibody (1:100), stained with DAPI (5 μg/mL), rinsed with PBS, and photographed with an inverted fluorescence microscope (TE2000U, Nikon, Japan).

2.13. Dual-luciferase reporter assay

Sirt1 3′UTR sequence was constructed and cloned into PMIR-RB-Report dual luciferin reporter vector to obtain Sirt1-WT and Sirt1-MUT plasmids. After co-transfection of the two Pmir-Sirt1 plasmids with the miR-138-5p mimic into BJ and HaCaT cells for 24 h, the fluorescence intensity of the reporter gene was detected.

2.14. miR-138-5p mimic transfection

The miR-138-5p mimic and mimic negative control were dissolved in serum-free medium and allowed to equilibrate for 5 min at room temperature. Each solution was then mixed with Lipofectamine2000. The solution was gently mixed for 20 min and left to form the mimicking liposomes. BJ cells were transfected with the transfection mixture in serum-free medium. After 6 h, the medium was replaced with fresh medium at 37 °C. The effects of the purslane extract on the mRNA and protein levels of the genes after transfection were measured.

2.15. miR-138-5p inhibitor and Sirt1 siRNA co-transformation test

Transfection solutions containing the miR-138-5p inhibitor and Sirt1 siRNA were obtained. The two solutions were gently mixed at 25 °C for 20 min. BJ cells were transfected with the transfection mixture in serum-free medium. The effects of the purslane extract on the mRNA and protein levels of the genes after co-transfection were measured.

2.16. Agomir transfection of miR-138-5p in mice

Twenty-eight mice were randomly divided into four groups (n = 7 each): agomir negative control (NC), agomir, agomir + UV radiation, and agomir + UV radiation + purslane extract (Pur). Mice in the agomir + UV radiation and agomir + UV radiation + Pur groups were exposed to UV light. Mice in the agomir and NC groups were administered an intradermal injection of miR-138-5p agomir (2.5 nmol/g/day) or the same dosage of agomir NC twice a week for 8 weeks. After modeling, the serum, tissue, and gene expression

Table 2
Antibody information.

Antibody	Source	Dilutions	Manufacturer
Sirt1	Rabbit	1:1000	Zenbio
p-65	Rabbit	1:1000	Proteintech
Cox2	Rabbit	1:2000	Proteintech
HMGB1	Rabbit	1:1000	Proteintech
Nrf2	Rabbit	1:1000	Proteintech
Keap1	Rabbit	1:1000	Zenbio
SOD	Rabbit	1:1000	Proteintech
HO-1	Rabbit	1:1000	Proteintech
GAPDH	Rabbit	1:5000	Proteintech
HRP-conjugated goat anti-rabbit	Affinipure IgG (H + L)	1:6000	Proteintech

levels in the signal were tested.

2.17. RNA extraction and RT-PCR detection

miRNA and mRNA samples were extracted according to the manufacturer's instructions. The purity and content of extracted RNA samples were calculated, and the samples were packaged and stored at −80 °C. Subsequently, the miRNA was synthesized, and the relative level of miR-138-5p was normalized to that of U6. For mRNAs analysis, cDNA was synthesized, and the relative levels were normalized to those of GAPDH. The relative quantification of miR-138-5p and mRNAs was performed using the $2^{-\Delta\Delta Cq}$ method. The corresponding primer sequences are listed in Table 1.

2.18. Western blotting assay

Protein samples were extracted according to the manufacturer's instructions and quantified using the BCA protein assay kit. The samples were loaded onto an SDS- PAGE gel for separation. The proteins were then transferred onto polyvinylidene fluoride membranes (Millipore, USA). The membranes were incubated with primary antibodies of Sirt1, p-65, Cox2, HMGB1, Nrf2, Keap1, SOD, HO-1, and GAPDH overnight, and then incubated with an HRP-conjugated secondary antibody. Protein levels were detected using a ChemiDoc™XRS Imaging System (Bio-Rad Laboratories, USA) and enhanced chemiluminescence. GAPDH was used as a loading control to normalize the relative protein levels. The corresponding antibody information is listed in Table 2.

2.19. Statistical analyses

Data obtained in this study were expressed as the mean ± standard deviation (SD). GraphPad 5.0 was used for analyses, and the significance level was set at $p < 0.05$. To determine whether there were significant differences among multiple groups, we used one-way ANOVA and Newman-Keuls methods for multiple comparisons. An unpaired *t*-test was used to compare two groups.

3. Results

3.1. Protective effect of purslane extract on UVB-induced cell damage

The results in Fig. 1A showed that Purslane extract at the concentration of 4800 ng/mL produced cytotoxicity to the cells, which showed no toxicity to BJ and HaCat cells at the concentrations of 150–600 ng/mL. Therefore, extracts at concentrations of 150, 300, and 600 ng/mL were selected for subsequent experiments. UVB irradiation was used to establish a cellular photoaging model. Under these conditions, purslane extract significantly reversed UVB-induced cell injury (Fig. 1A). As shown in Fig. 1B, the green fluorescence in UVB-induced model groups was significantly increased, which was markedly attenuated by the extract. As shown in Fig. 1C, compared with control groups, the mRNA levels of ICAM-1, IL-1, IL-6, and TNF-α in UVB groups were markedly raised, and these were also reversed by the extract.

3.2. Protective effect of purslane extract on skin photoaging in mice

Compared to the control group, the mice in the model group showed visible wrinkles, pigmentation, skin keratinization, dilated capillaries, and dry skin, all of which were improved by the purslane extract, and the increased pigment spots caused by UV radiation were also improved (Fig. 2A). HE staining (Fig. 2B) showed that the epidermis and dermis of mice in the model group were swollen and thickened compared to those in the control group. Compared with the model group, the dermal fibers in the positive control group and medium- and high-dose purslane extract groups were closely arranged to improve abnormal epidermal thickening. Masson's trichrome staining demonstrated that the collagen fibers in the dermal tissue of the model group were loose with uneven distribution and local collagen fibers, which were reverted to nearly normal by the extract. Toluidine blue staining (Fig. 2B) showed that mast cells were clearly observed in the model group, and were decreased by the extract. The data in Fig. 2C show that the serum HYP, HA, CoLI, CAT,

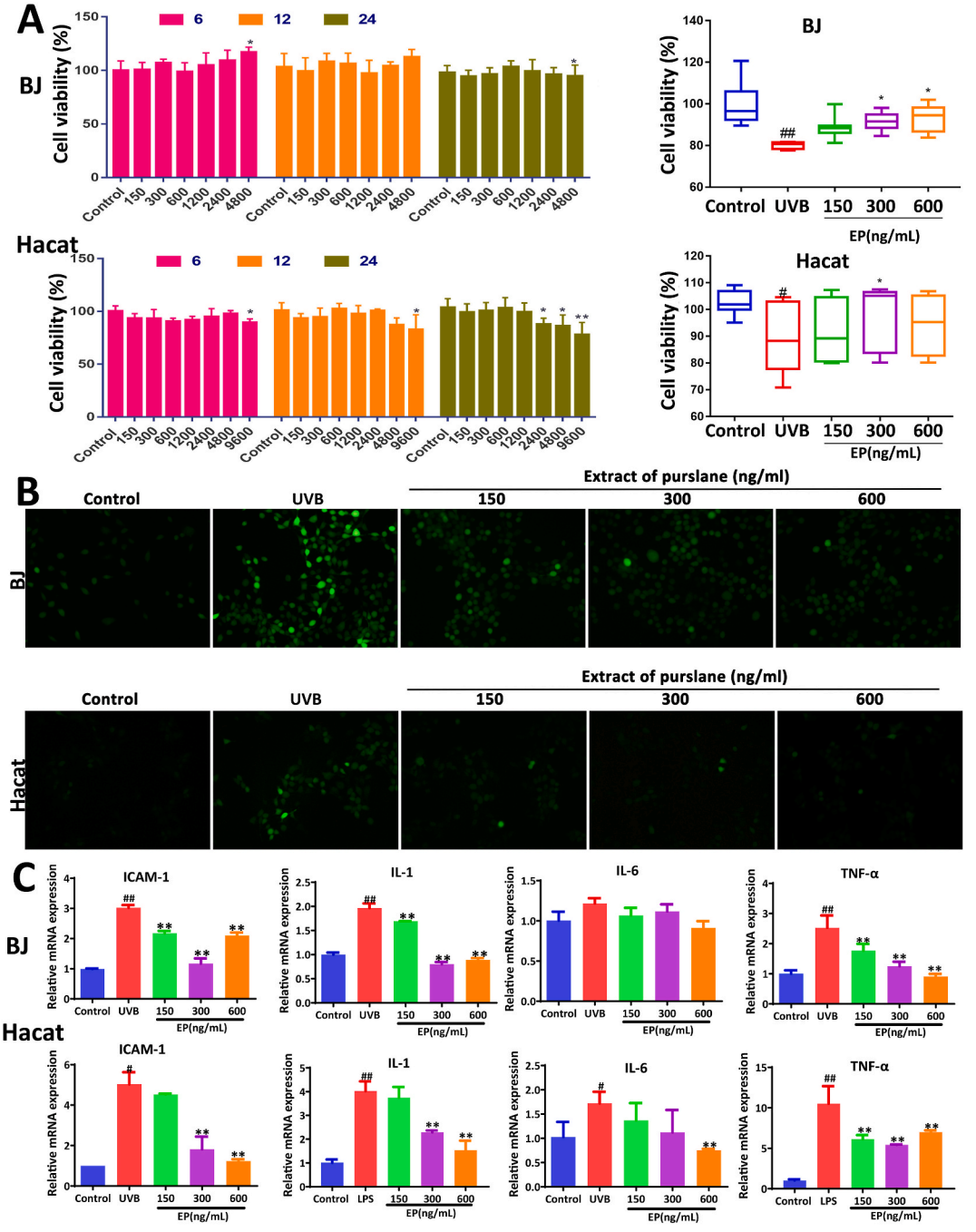

Fig. 1. Effects of purslane extract on protecting against UVB-induced BJ and HaCat cell injury. (A) Cytotoxicity of the extract on UVB-induced injury and the effects of the extract on cell viability. (B) Effects of purslane extract on ROS levels in UVB-induced BJ and HaCat cells. (C) Effects of purslane extract on ICAM-1, IL-1, IL-6, and TNF-α levels in cells. $^{\#}p < 0.05$ and $^{\#\#}p < 0.01$ compared with control groups; $^{*}p < 0.05$ and $^{**}p < 0.01$ compared with control or model groups (n = 6).

and T-SOD levels in the model group were markedly decreased, and MDA levels were increased compared to those in the control group, which were all significantly reversed by the purslane extract. Concurrently, the levels of HA, COLI, CAT, MDA, and T-SOD in the high-dose group were comparable to those in the VE group. Due to its strong antioxidant capacity, VE protects against skin damage caused by UV radiation. These results showed that high doses of the purslane extract had antioxidant capacities comparable to those of VE.

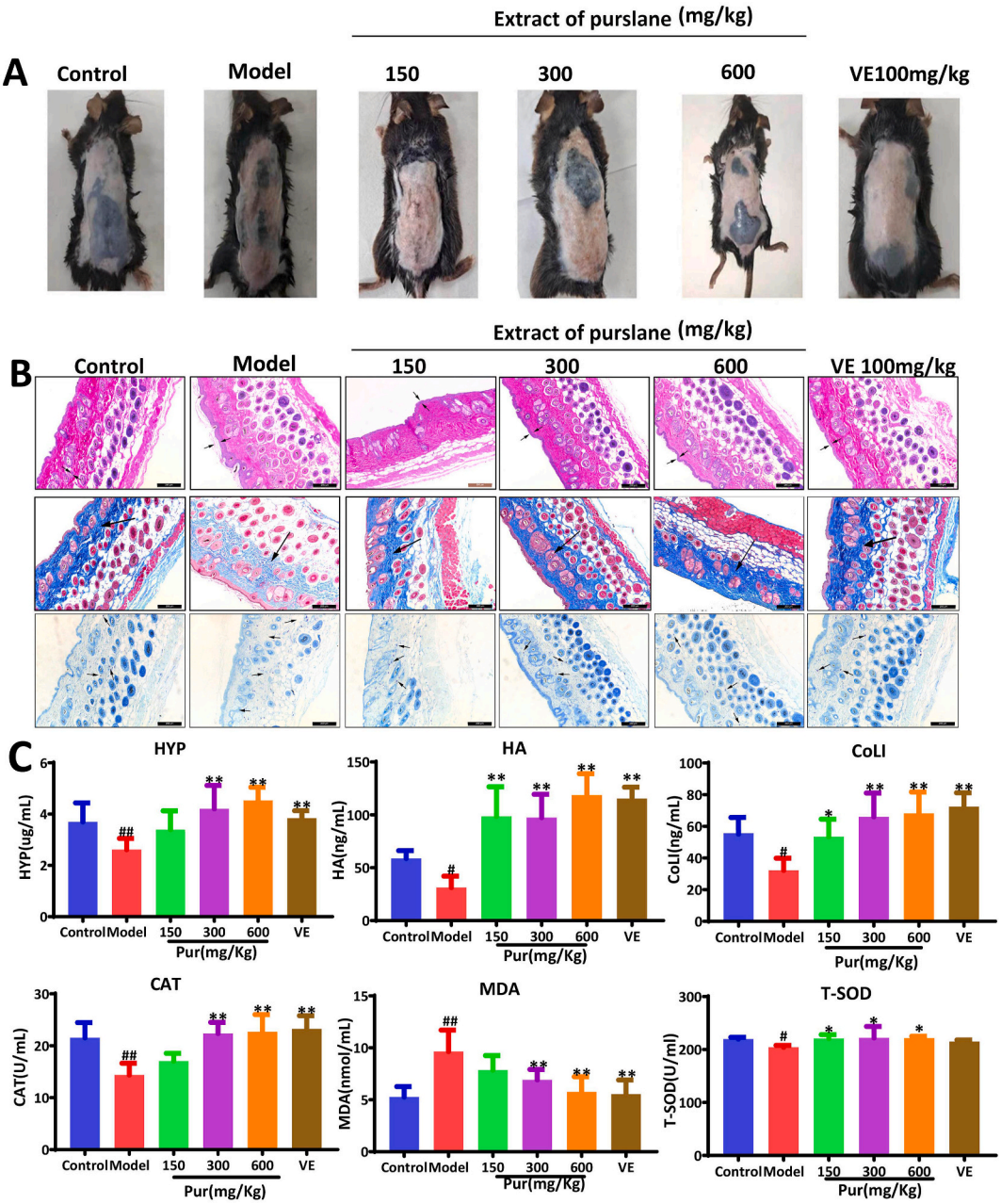

Fig. 2. Effects of purslane extract on protecting against UV-induced skin injury in mice. (A) Purslane extract improved UV-induced skin appearance in mice. (B) Effects of purslane extract on UV-induced skin injury based on HE, Masson's and toluidine blue sections. (C) Effects of purslane extract on the levels of HYP, HA, COLL, CAT, MDA, and T-SOD of mice induced by UV radiation. $^{\#}p < 0.05$ and $^{\#\#}p < 0.01$ compared with control group; $^{*}p < 0.05$ and $^{**}p < 0.01$ compared with model group (n = 6).

3.3. Purslane extract regulates miR-138-5p/Sirt1 signal in vitro

The FISH results showed that miR-138-5p was highly expressed in the cytoplasm. The expression levels of miR-138-5p increased and Sirt1 levels decreased in UVB-treated cells (Fig. 3A–B), and these effects were reversed by the extract. The data in Fig. 3C show that the levels of miR-138-5p were significantly increased in UVB- induced cells and decreased by the extract. The protein levels of p-65, Cox2, HMGB1, and Keap1 were significantly increased in UVB-treated cells, whereas the protein levels of Sirt1, Nrf2, HO-1, and SOD were significantly decreased, all of which were reversed by the extract. The mRNA levels of GCLC, GCLM, and NQO-1 were decreased in UVB-treated cells and were significantly increased by 600 ng/mL of the extract (Fig. 3D–E).

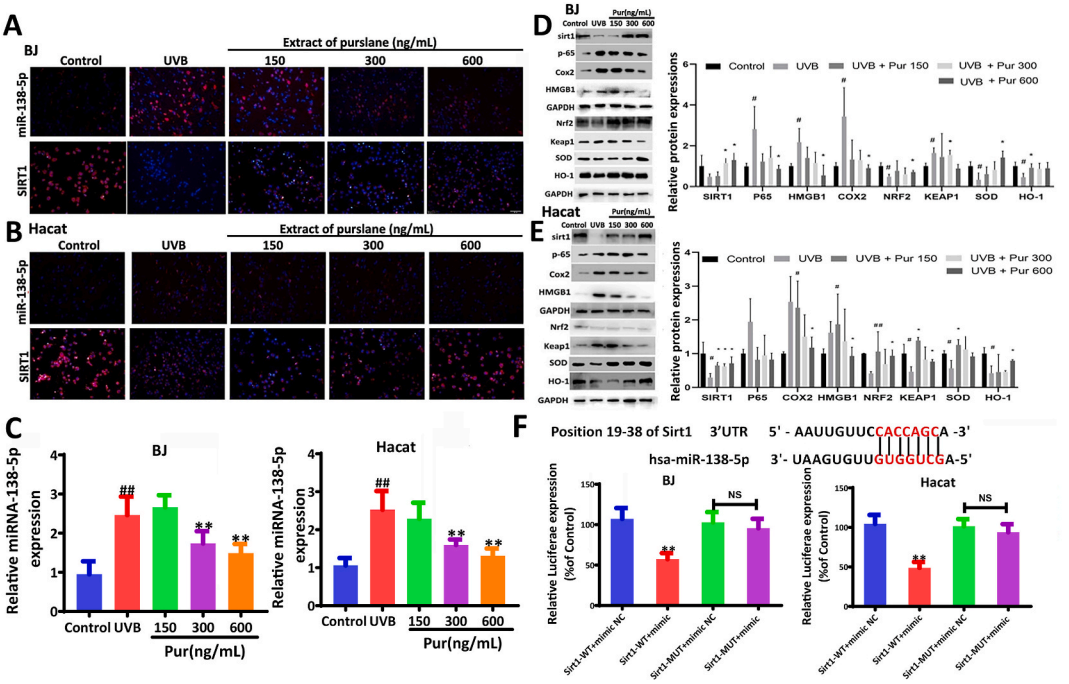

Fig. 3. Effects of purslane extract on miR-138-5p and Sirt1 levels in cells. (A) Effect of the purslane extract on the levels of miR-138-5p and Sirt1 in BJ cells based on Fish and immunofluorescence assays. (B) Effect of purslane extract on the levels of miR-138-5p and Sirt1 in HaCat cell based on Fish and immunofluorescence assays. (C) The expression levels of miR-138-5p in BJ and HaCat cells after administration based on real-time PCR assay. (D–E) Effect of purslane extract of on the protein and/or mRNA levels of Sirt1, p-65, Cox2, HMGB1, Nrf2, Keap1, SOD, HO-1, IL-1, IL-6, ICAM-1, TNF-α, GCLM, GCLC, and NQO1 in BJ and HaCat cells (the original bands were shown in Figs. S1 and S2 in supplementary material). (F) Relative luciferase expression with Sirt1 3′-UTR after co-transfection with miR-138-5p mimic or NC in BJ and HaCat cells. $^{\#}p < 0.05$ and $^{\#\#}p < 0.01$ compared with control group; $^{**}p < 0.01$ compared with Sirt1-WT + mimic NC or model group (n = 3).

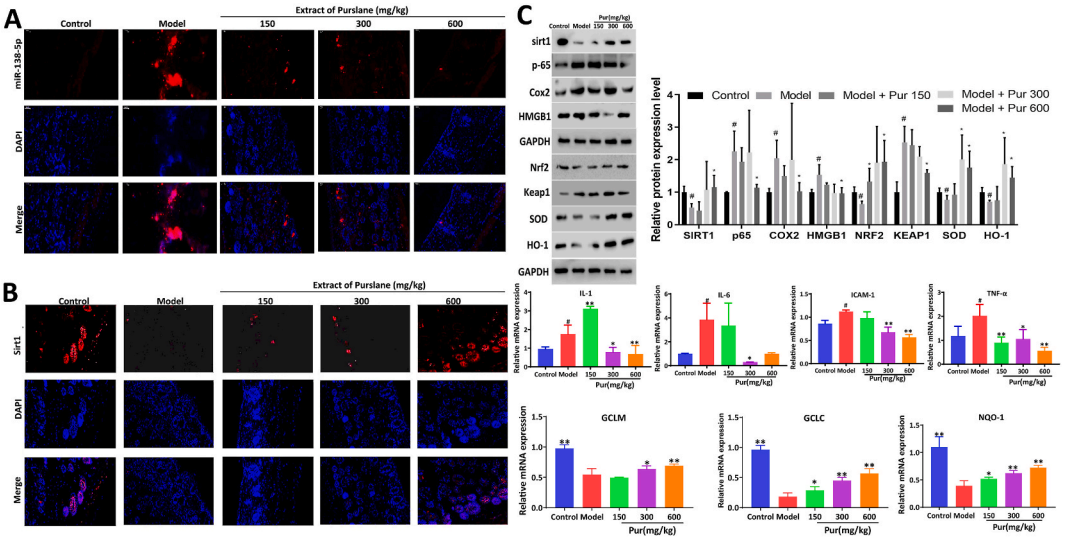

Fig. 4. Effects of purslane extract on miR-138-5p and Sirt1 levels in mice. (A–B) Effect of purslane extract on the levels of miR-138-5p and Sirt1 in mice based on Fish and immunofluorescence assays. (C) Effect of purslane extract on the protein and/or mRNA levels of sirt1, p-65, Cox2, HMGB1, Nrf2, Keap1, SOD, HO-1, IL-1, IL-6, ICAM-1, TNF-α, GCLM, GCLC, and NQO1 (the original bands were shown in Fig. S3 in supplementary material). $^{**}p < 0.01$ compared with model group (n = 3).

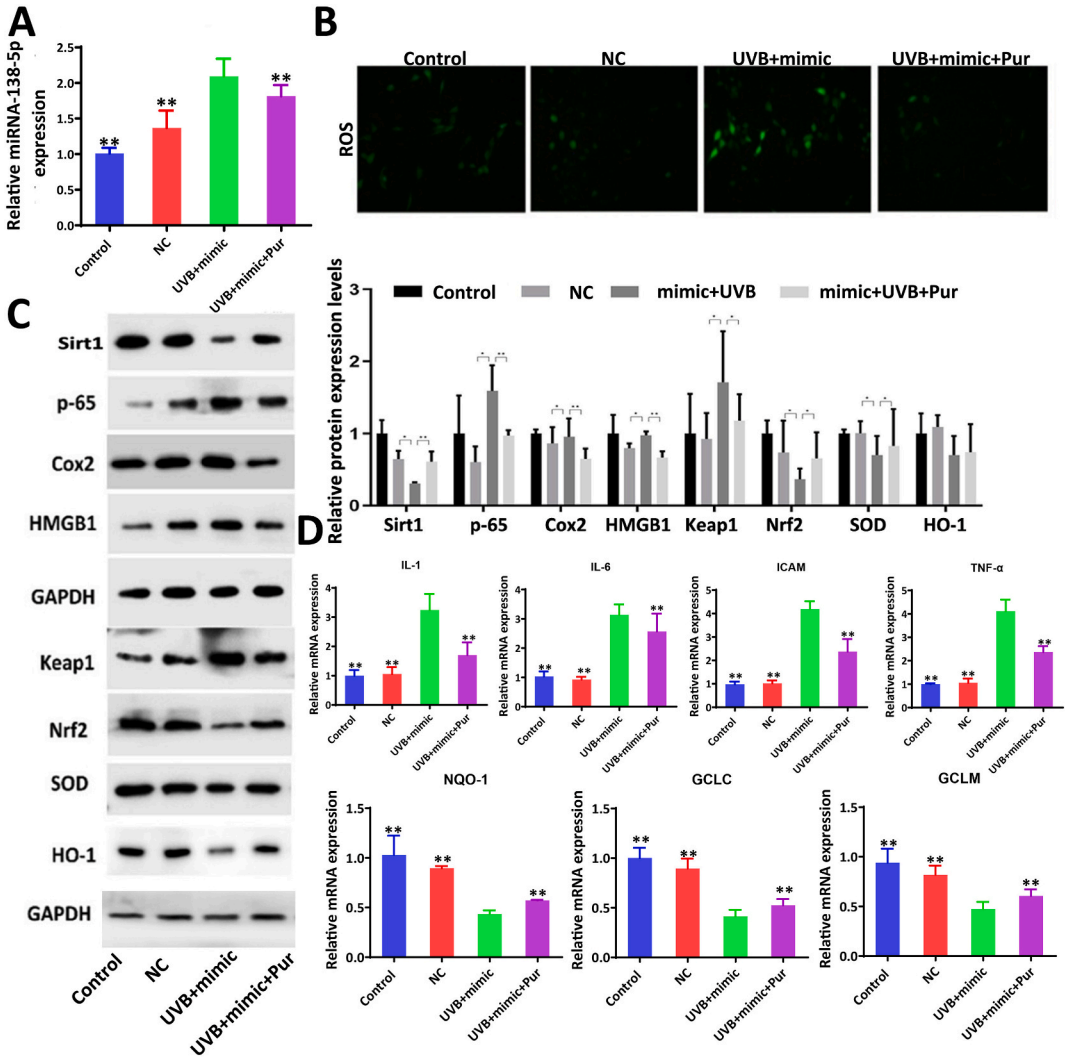

Fig. 5. MiR-138-5p mimic affected the effect of purslane extract in UVB-induced cell damage. (A) Effects of purslane extract on miR-138-5p expression level after miR- 138-5p mimic transfection (n = 6). (B) Expression levels of ROS in cells treated with purslane extract after transfection of miR-138-5p mimic (n = 3). (C–D) Expression levels of Sirt1, p-65, Cox2, HMGB1, Nrf2, Keap1, SOD, HO-1, IL-1, IL-6, ICAM-1, TNF-α, GCLM, GCLC, and NQO1 in the cells treated with the extract after transfection of miR-138-5p inhibitor (n = 3), (the original bands were shown in Fig. S4 in supplementary material). Data are expressed as the mean ± SD. **p < 0.01 compared with UVB + mimic group.

3.4. miR-138-5p directly targets Sirt1

The binding site between Sirt1 3′UTR mRNA and miR-138-5p is shown in Fig. 3F. Dual-luciferase reporter assay confirmed that the relative fluorescence intensity of the Sirt1-WT + mimic group was significantly lower than that of the Sirt1-WT + mimic NC group. However, this effect was not observed in the mutated Sirt1 group, indicating that Sirt1 has a specific binding site for miR-138-5p.

3.5. Purslane extract regulates miR-138-5p/Sirt1 signal in vivo

The fluorescence intensity of miR-138-5p was significantly increased in model mice and was decreased by the extract, indicating that the extract reduced miR-138-5p expression in mouse skin under UV radiation (Fig. 4A). The fluorescence intensity of Sirt1 was downregulated in the model group and was significantly increased by the extract (Fig. 4B). Subsequently, the mRNA levels of ICAM-1, IL-6, IL-1, and TNF-α were significantly increased in model group, and were significantly downregulated in treatment group. In addition, the mRNA levels of GCLM, GCLC, and NQO-1 in the model mice significantly decreased and were gradually reversed after treatment administration. The protein levels of p-65, Cox2, HMGB1, and Keap1 were significantly increased, whereas the protein levels of Nrf2, HO-1, and SOD were significantly decreased, all of which were reversed by the extract (Fig. 4C).

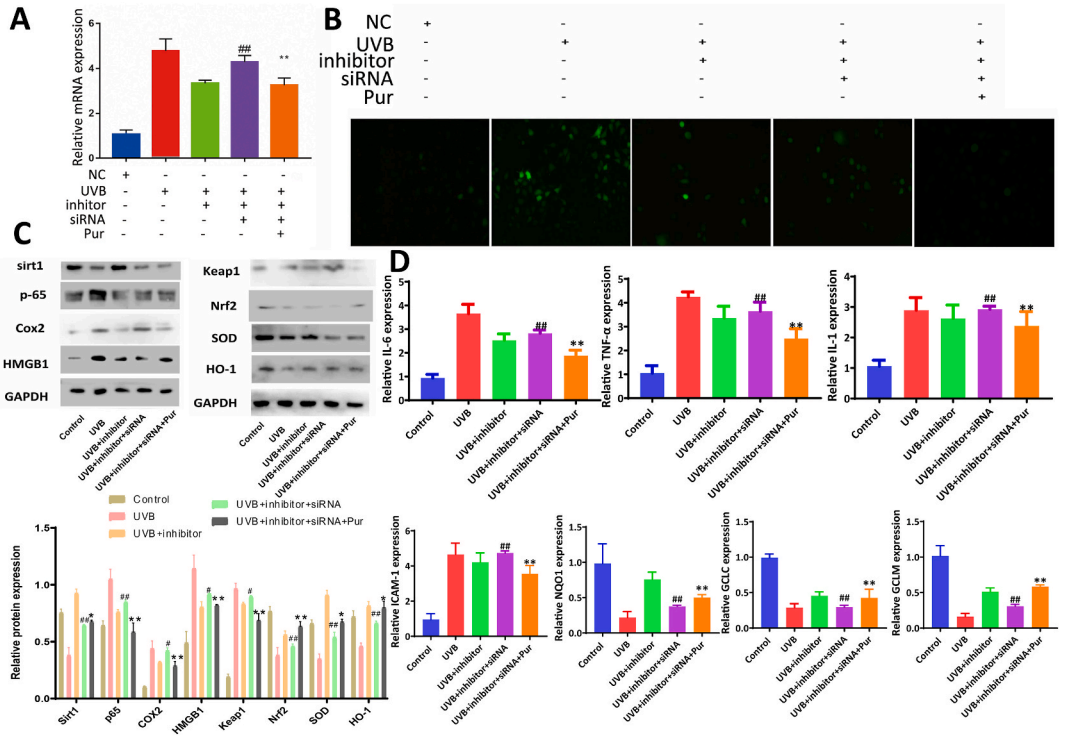

Fig. 6. MiR-138-5p inhibitor and Sirt1 siRNA affected the effects of purslane extract in UVB-induced cell damage. (A) Effects of purslane extract on miR-138-5p expression level after miR-138-5p inhibitor and Sirt1 siRNA transfection (n = 6). (B) Expression levels of ROS in the cells treated with purslane extract after transfection of miR-138-5p inhibitor and Sirt1 siRNA (n = 3). (C–D) Expression levels of Sirt1, p-65, Cox2, HMGB1, Nrf2, Keap1, SOD, HO-1, IL-1, IL-6, ICAM-1, TNF-α, GCLM, GCLC, and NQO1 in cells treated with purslane extract after transfection of miR-138-5p inhibitor and Sirt1 siRNA (n = 3), (the original bands were shown in Fig. S5 in supplementary material). Data are expressed as the mean ± SD. $^{\#\#}p < 0.01$ compared with UVB + inhibitor group; $^{**}p < 0.01$ compared with UVB + inhibitor + sirt1 siRNA group.

3.6. Overexpression miR-138-5p affects the effects of the extract on UVB-induced cell damage

As shown in Fig. 5A, compared to the UVB + mimic group (miR-138-5p mimic transfection), miR-138-5p levels were significantly decreased, and ROS levels were significantly downregulated in the UVB + mimic + Pur group (Fig. 5B). Compared to the NC group (mimic negative control transfection), the protein levels of Sirt1, Nrf2, HO-1, and SOD were significantly downregulated, and the levels of COX2, p-65, HMGB1, and Keap1 were significantly upregulated in the UVB + mimic group, which was gradually reversed in the UVB + mimic + Pur group (Fig. 5C). As shown in Fig. 5D, compared with UVB + mimic group, the mRNA levels of IL-1, IL-6, ICAM-1, and TNF-α were significantly downregulated, whereas the levels of NQO1, GCLC and GCLM were significantly upregulated by the extract in UVB + mimic + Pur group.

3.7. Co-transfection of miR-138-5p inhibitor and si-Sirt1 affects the effects of the extract on UVB-induced cell damage

As shown in Fig. 6A, compared to the UVB group, the miR-138-5p level was significantly decreased in the UVB + inhibitor group, which was significantly upregulated in the UVB + inhibitor + siRNA group and downregulated by the extract. ROS levels also showed the same trend in each group (Fig. 6B). As shown in Fig. 6C, compared to the UVB group, the expression levels of Sirt1, Nrf2, HO-1, and SOD were significantly upregulated and the levels of p-65, HMGB1, and Keap1 were significantly downregulated in the UVB + inhibitor group. These levels were significantly reduced in the UVB + inhibitor + siRNA group. However, compared with the UVB + inhibitor + siRNA group, the protein levels were significantly reversed in the UVB + inhibitor + siRNA + Pur group. As shown in Fig. 6D, compared with UVB group, the mRNA levels of IL-1, IL-6, ICAM-1, and TNF-α were significantly downregulated in UVB + inhibitor group, and the levels of NQO1, GCLC, and GCLM were significantly upregulated. These effects were reversed when miR-138-5p and Sirt1 were co-inhibited. However, the expression levels of genes and proteins were reversed after administration of the purslane extract.

3.8. Overexpression of miR-138-5p aggravates UV radiation-induced skin photoaging and affects the effectiveness of purslane extract in mice

Based on these observations, the mice in the Agomir and Agomir + model groups had significant folds and severe skin thickening

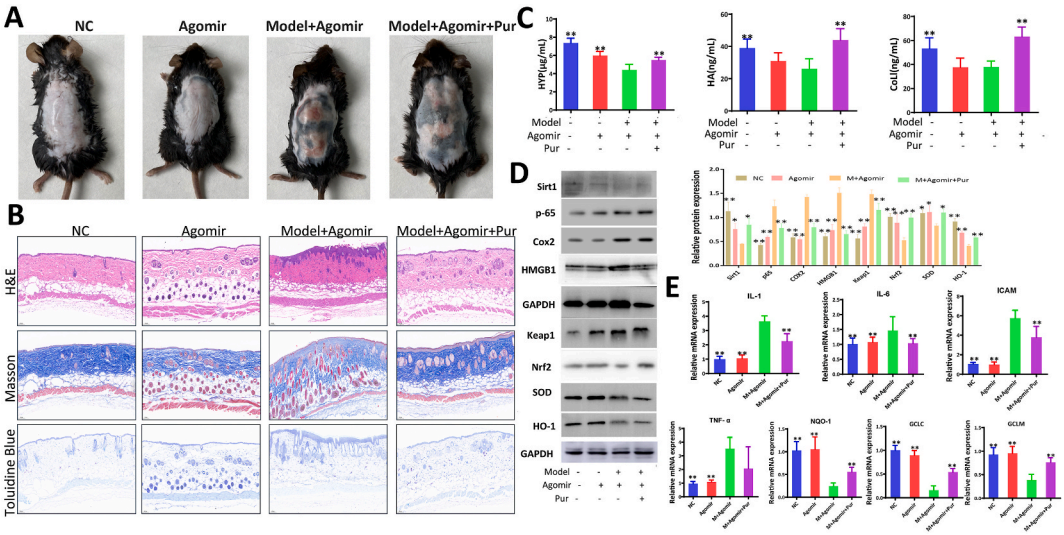

Fig. 7. Effects of purslane extract on protecting UV-induced skin injury in mice after Agomir transfection. (A) Effects of purslane extract on UV-induced skin appearance after Agomir transfection in mice. (B) Effects of purslane extract on skin injury based on HE, Masson's and toluidine blue staining after Agomir transfection. (C) Effects of the extract on levels of HYP, HA, and COLI of mice induced by UV after Agomir transfection. (D) Expression levels of Sirt1, p-65, Cox2, HMGB1, Nrf2, Keap1, SOD, and HO-1.(E) Expression levels of IL-1, IL-6, ICAM-1, TNF-α, GCLM, GCLC, and NQO1 in mice treated with purslane extract after transfection of Agomir. $^{**}p < 0.01$ compared with model + Agomir group (n = 3), (the original bands were shown in Fig. S6 in supplementary material).

compared to those in the NC group. Mice in the Agomir + model group showed pigmentation, rough and dry surfaces, telangiectasia, and evidence of skin damage, which were reversed by the extract (Fig. 7A). Fig. 7B shows that the mice injected with Agomir and UV radiation had characteristics of dermal injury, collagen fiber distortion and fracture, and the skin barrier injury of mast cells was increased, which was improved by the extract. Fig. 7C shows that compared to the Agomir + Model group, the levels of HA, HYP, and COL1 in the Agomir + Model + Pur group were significantly increased. Western blotting results showed that, compared to the Model + Agomir group, the expression levels of Sirt1, Nrf2, HO-1, and SOD were significantly increased, and the levels of P65, COX2, HMGB1, and Keap1 were significantly downregulated in the Model + Agomir + Pur group (Fig. 7D). As shown in Fig. 7E, compared with the Model + Agomir group, the mRNA levels of IL-1, IL-6, ICAM-1, and TNF-α were downregulated, and the levels of NQO1, GCLC, and GCLM were significantly upregulated in the Model + Agomir + Pur group.

4. Discussion

The skin, as a necessary interface between the internal and external environments, also ages with time, similar to other organs [36]. Fighting skin photoaging, which is a type of skin damage induced by UV radiation [37], has become a major focus of research in recent years. Exposure to ultraviolet light can trigger the production and accumulation of ROS in skin cells, thereby increasing oxidative stress and leading to photoaging [3]. In addition, ROS play an important role in the progression of inflammatory disorders [10]. Mitochondrial-derived ROS (MtROS) can contribute to the UVB-mediated production of pro-inflammatory cytokines [38]. In the present study, UVB-induced BJ and HaCat cells showed ROS accumulation and the levels of ICAM-1, IL-1, IL-6, and TNF-α were increased in model cells. In addition, we found that the skin of UV-treated mice showed significant skin barrier damage and loose collagen fibers. HA and COLI, as indicators of skin aging, and HA, which keeps the skin moisturized, smooth, and delicate, were also detected. UV irradiation increased the number of mast cells with abnormal levels of HYP, HA, and COLI, as confirmed in a previous report [39].

In recent years, the cosmetics industry has been interested in identifying naturally occurring bioactive compounds that protect against skin damage. Luteolin, an active natural ingredient with antioxidant and anti-inflammatory properties, protects against skin damage induced by UV radiation [40]. Previous studies have shown that pterostilbene inhibits UVB-induced keratinocyte photodamage [41]. Neochlorogenic acid regulates the production of MMP-1 and procollagen type I and protects fibroblasts and keratinocytes from UVB irradiation [42]. Therefore, in this study, we aimed to identify herbal extracts with anti-inflammatory and anti-oxidative activities to improve skin photoaging caused by UV radiation.

Purslane has antioxidant and anti-inflammatory activities that can significantly reduce CCI-induced neuropathic pain in rats [43]. In UV-induced mouse models, the purslane extract significantly reversed the UV-induced changes in MDA, T-SOD, and CAT levels, which are indicators of oxidative stress. T-SOD plays a crucial role in the balance between oxidative and antioxidative processes and can remove superoxide anion radicals to protect cells from damage. MDA levels reflect the degree of lipid peroxidation and cell damage in the body. CAT is an enzyme scavenger that removes hydrogen peroxide from the body and is a key enzyme in biological defense systems. The pathological profile also showed that the extract was effective in improving abnormal epidermal thickening caused by UV

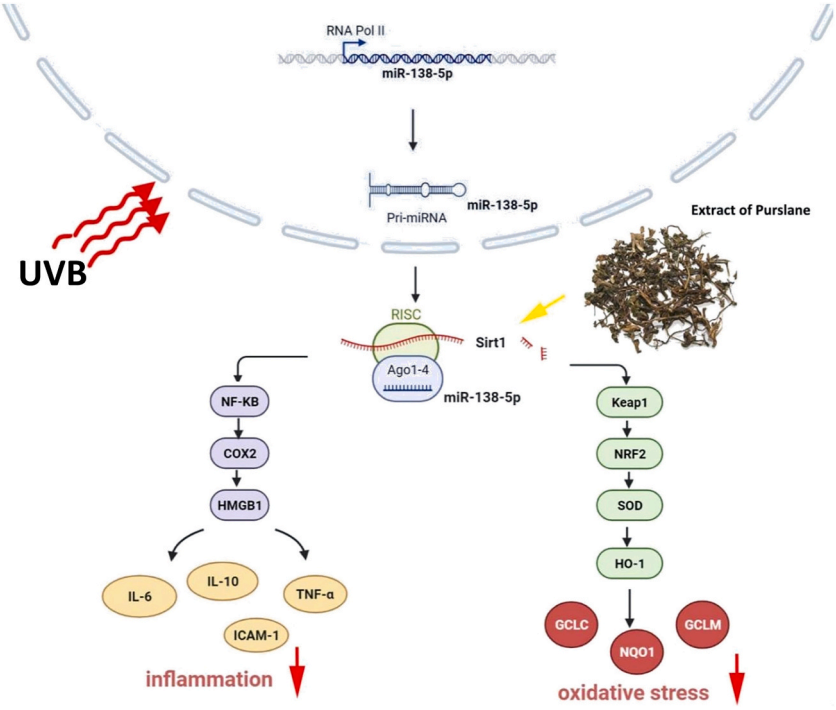

Fig. 8. Schematic summary of the effects of purslane extract against UV-induced skin photoaging by regulating miR-138-5p/Sirt1 signaling.

radiation, reducing mast cells, and aligning collagen fibers in the skin tissue. HYP, HA, and COL1 were also restored. *In vitro*, the levels of ICAM-1, IL-1, IL-6, and TNF-α were decreased after administration of the extract in UVB-induced cells. Therefore, the purslane extract showed significant antioxidative and anti-inflammatory effects against UV-induced skin damage.

It has been shown that reducing the expression level of miR-138-5p can induce OVA-induced airway hyperreactivity and inflammation, as well as improve lung inflammatory infiltration and mucus [44]. Sirt1, a member of the silent information regulator protein complex family, plays a vital role in inflammation by regulating nuclear factor kappa B (NF-κB) and activator protein 1 (AP-1) [45]. We observed high levels of miR-138-5p and low levels of Sirt1 in UVB-treated cells and mice. Subsequently, we demonstrated that miR-138-5p can target 3′UTR of Sirt1 to inhibit its expression. The expression of miR-138-5p was significantly reduced by the extract. When miR-138-5p was overexpressed, oxidative stress and inflammation worsened. When purslane extract was administered, miR-138-5p levels were reduced to improve oxidative stress and inflammation. These results were confirmed both *in vivo* and *in vitro*. We inhibited the expression of miR-138-5p in UVB-induced BJ cells, and the results showed that UVB-induced damage was significantly improved. When Sirt1 was simultaneously inhibited, UVB-induced damage was aggravated, indicating that the damage was caused by the inhibition of Sirt1 through the overexpression of miR-138-5p. Interestingly, when miR-138-5p and Sirt1 were co-inhibited, the purslane extract still reduced miR-138-5p as well as the indices of oxidative stress and inflammation, suggesting that the purslane extract had regulatory effects by regulating the upstream genes of miR-138-5p.

Purslane is a highly nutritious plant with significant nutraceutical and pharmacological potentials. This study showed the potent protective effects of purslane extract against UV-induced skin photoaging via regulation of the miR-138-5p/Sirt1 axis, as summarized in Fig. 8. However, further investigations on purslane and its additional pharmacological activities and mechanisms are needed.

Funding

The authors gratefully acknowledge funding from the Spring City Plan: The High-Level Talent Promotion and Training Project of Kunming (2022SCP008) and the Independent Research Fund of the Yunnan Characteristic Plant Extraction Laboratory (2022YKZY001).

Ethical approval and consent to participate

Male C57BL/6J mice were obtained from the Experimental Animal Center of Dalian Medical University, Dalian, China (SCXK (Liao) 2013-0003).

Data availability statement

Data associated with study were not deposited into a publicly available repository. Data will be made available on request from the corresponding author.

CRediT authorship contribution statement

Liping Qu: Formal analysis, Investigation, Methodology, Project administration, Resources, Supervision, Validation, Writing – review & editing. **Feifei Wang:** Investigation, Methodology, Supervision. **Xiao Ma:** Data curation, Formal analysis, Project administration, Writing – original draft.

Declaration of competing interest

The authors declare that they have no known competing financial interests or personal relationships that could have appeared to influence the work reported in this paper.

Acknowledgments

Not applicable.

Appendix A. Supplementary data

Supplementary data to this article can be found online at https://doi.org/10.1016/j.heliyon.2023.e21955.

References

[1] D.J. Tobin, Introduction to skin aging, J. Tissue Viability 26 (1) (2017) 37–46.
[2] M.A. Farage, K.W. Miller, P. Elsner, H.I. Maibach, Intrinsic and extrinsic factors in skin ageing: a review, Int. J. Cosmet. Sci. 30 (2) (2008) 87–95.
[3] G. Petruk, R. Del Giudice, M.M. Rigano, D.M. Monti, Antioxidants from plants protect against skin photoaging, Oxid. Med. Cell. Longev. 2 (2018), 1454936, 2018.
[4] Y. Ke, X.J. Wang, TGFβ signaling in photoaging and UV-induced skin cancer, J. Invest. Dermatol. 141 (4S) (2021) 1104–1110.
[5] G.J. Fisher, S. Kang, J. Varani, Mechanisms of photoaging and chronological skin aging, Arch. Dermatol. 138 (11) (2002) 1462–1470.
[6] E. Bang, D.H. Kim, H.Y. Chung, Protease-activated receptor 2 induces ROS- mediated inflammation through Akt-mediated NF-κB and FoxO6 modulation during skin photoaging, Redox Biol. 44 (2021), 102022.
[7] J.E. Oh, M.S. Kim, W.K. Jeon, Y.K. Seo, B.C. Kim, J.H. Hahn, C.S. Park, A nuclear factor kappa B-derived inhibitor tripeptide inhibits UVB-induced photoaging process, J. Dermatol. Sci. 76 (3) (2014) 196–205.
[8] Y. Yu, S. Dunaway, J. Champer, J. Kim, A. Alikhan, Changing our microbiome: probiotics in dermatology, Br. J. Dermatol. 182 (1) (2020) 39–46.
[9] R. Kang, R. Li, P. Dai, Z. Li, Y. Li, C. Li, Deoxynivalenol induced apoptosis and inflammation of IPEC-J2 cells by promoting ROS production, Environ. Pollut. 251 (2019) 689–698.
[10] M. Mittal, M.R. Siddiqui, K. Tran, S.P. Reddy, A.B. Malik, Reactive oxygen species in inflammation and tissue injury, Antioxid. Redox Signal. 20 (7) (2014) 1126–1167.
[11] Y. Gu, J. Han, C. Jiang, Y. Zhang, Biomarkers, oxidative stress and autophagy in skin aging, Ageing Res. Rev. 59 (2020), 101036.
[12] N. Bushati, S.M. Cohen, microRNA functions, Annu. Rev. Cell Dev. Biol. 23 (2007) 175–205.
[13] D. Fu, W. Yu, M. Li, H. Wang, D. Liu, X. Song, Z. Li, Z. Tian, MicroRNA- 138 regulates the balance of Th1/Th2 via targeting RUNX3 in psoriasis, Immunol. Let. 166 (1) (2015) 55–62.
[14] Gerasymchuk, M.; Cherkasova, V.; Kovalchuk, O.; Kovalchuk, I. The role of microRNAs in organismal and skin aging. Int. J. Mol. 25;21(15):5281.
[15] Y.Y. Xiao, P.J. Fan, S.R. Lei, M. Qi, X.H. Yang, MiR-138/peroxisome proliferator-activated receptor β signaling regulates human hypertrophic scar fibroblast proliferation and movement in vitro, J. Dermatol. 42 (5) (2015) 485–495.
[16] S. Nama, M. Muhuri, F.D. Pascale, S. Quah, L. Aswad, M. Fullwood, P. Sampath, MicroRNA-138 is a prognostic biomarker for triple-negative breast cancer and promotes tumorigenesis via TUSC2 repression, Sci. Rep. 9 (1) (2019), 12718.
[17] C. Wang, X. Sun, Z. Qiu, A. Chen, MiR-138-5p exacerbates hypoxia/reperfusion -induced heart injury through the inactivation of SIRT1-PGC-1α, Inflamm. Res. 68 (10) (2019) 867–876.
[18] S. Tian, X. Guo, C. Yu, C. Sun, J. Jiang, miR-138-5p suppresses autophagy in pancreatic cancer by targeting SIRT1, Oncotarget 8 (7) (2017) 11071–11108.
[19] Y. Yang, Y. Liu, Y. Wang, Y. Chao, J. Zhang, Y. Jia, J. Tie, D. Hu, Regulation of SIRT1 and its roles in inflammation, Front. Immunol. 13 (2022), 831168.
[20] A. Kauppinen, T. Suuronen, J. Ojala, K. Kaarniranta, A. Salminen, Antagonistic crosstalk between NF-κB and SIRT1 in the regulation of inflammation and metabolic disorders, Cell. Signal. 25 (10) (2013) 1939–1948.
[21] J. Li, X. Zeng, X. Yang, H. Ding, Lycopene ameliorates skin aging by regulating the insulin resistance pathway and activating SIRT1, Food Funct. 13 (21) (2022) 11307–11320.
[22] M. An, H. Kim, J.M. Moon, H.S. Ko, P. Clayton, Y.H. Lim, Enzyme -treated Zizania latifolia ethanol extract protects from UVA irradiation-induced wrinkle formation via inhibition of lysosome exocytosis and reactive oxygen species generation, Antioxidants 9 (10) (2020) 912.
[23] M. Ledrhem, M. Nakamura, M. Obitsu, K. Hirae, J. Kameyama, H. Bouamama, C. Gadhi, Y. Katakura, Essential oils derived from Cistus species activate mitochondria by inducing SIRT1 expression in human keratinocytes, leading to senescence inhibition, Molecules 27 (7) (2022) 2053.
[24] E.S. Elkhayat, S.R. Ibrahim, M.A. Aziz, Portulene, a new diterpene from Portulaca oleracea L, J. Asian Nat. Prod. Res. 10 (11–12) (2008) 1039–1043.
[25] U.R. Palaniswamy, B.B. Bible, R.J. McAvoy, Effect of nitrate: ammonium nitrogen ratio on oxalate levels of purslane, Trends New Crops New Uses 11 (2002) 453–455.
[26] R. Jin, Z.J. Lin, C.M. Xue, B. Zhang, Improved association-mining research for exploring Chinese herbal property theory: based on data of the Shennong's Classic of Materia Medica, J. Integr. Med. 11 (5) (2013) 352–365.

[27] L. Miao, H. Tao, Y. Peng, S. Wang, Z. Zhong, H. El-Seedi, S. Dragan, G. Zengin, W.S. Cheang, Y. Wang, J. Xiao, The anti-inflammatory potential of Portulaca oleracea L. (purslane) extract by partial suppression on NF-κB and MAPK activation, Food Chem. 290 (2019) 239–245.
[28] V. Baradaran Rahimi, H. Rakhshandeh, F. Raucci, B. Buono, R. Shirazinia, A. Samzadeh Kermani, F. Maione, N. Mascolo, V.R. Askari, Anti-inflammatory and anti-oxidant activity of portulaca oleracea extract on LPS-induced rat lung injury, Molecules 24 (1) (2019) 139.
[29] Y.L. Yuan, L.P. Qu, F.F. Wang, X. Ma, S.Y. Gao, Z.Y. Guo, Preparation Method and Application of Purslane Extract, 2019, CN110201012B.
[30] F.F. Wang, Y.L. Yuan, L.P. Qu, Determination of adenosine in Portulaca oleracea L. by high performance liquid chromatography, J. Food Saf. Qual. 11 (14) (2020) 4625–4630.
[31] N. Percie du Sert, V. Hurst, A. Ahluwalia, S. Alam, M.T. Avey, M. Baker, W.J. Browne, A. Clark, I.C. Cuthill, U. Dirnagl, M. Emerson, P. Garner, S.T. Holgate, D. W. Howells, N.A. Karp, S.E. Lazic, K. Lidster, C.J. MacCallum, M. Macleod, E.J. Pearl, H. Würbel, The ARRIVE guidelines 2.0: updated guidelines for reporting animal research, PLoS Biol. 177 (16) (2020) 3617–3624.
[32] Zhongmin Zhang, Yunling Xu, Ruicheng Lai, Huiyuan Deng, Fengling Zhou, Peiyan Wan, Xiubing Pang, Guoxin Huang, Xin Chen, Haoge Lin, Yong Lin, Zhenxing Che, Lin Jiang, Protective effect of the pearl extract from pinctada fucata martensii dunker on UV-induced photoaging in mice, Chem. Biodivers. 19 (3) (2022), e202100876.
[33] Young-In Kim, Won-Seok Oh, Phil Hyun Song, Sungho Yun, Young-Sam Kwon, Young Joon Lee, Sae-Kwang Ku, Chang-Hyun Song, Tae-Ho Oh, Anti-photoaging effects of low molecular-weight fucoidan on ultraviolet B-irradiated mice, Mar. Drugs 16 (8) (2018) 286.
[34] Bo Song, Dasong Liu, Tristan C. Liu, Kexin Li, Sai Wang, Jianguo Liu, Joe M. Regenstein, Yuxuan Wu, Peng Zhou, The combined effect of commercial tilapia collagen peptides and antioxidants against UV-induced skin photoaging in mice, Food Funct. 14 (13) (2023) 5936–5948.
[35] Laura Rojas Lorz, Byong Chul Yoo, Mi-Yeon Kim, Jae Youl Cho, Anti-wrinkling and anti-melanogenic effect of pradosia mutisii methanol extract, Int. J. Mol. Sci. 20 (5) (2019) 1043.
[36] T.K. Lin, L. Zhong, J.L. Santiago, Anti-inflammatory and skin barrier repair effects of topical application of some plant oils, Int. J. Mol. Sci. 19 (1) (2017) 70.
[37] F. Poon, S. Kang, A.L. Chien, Mechanisms and treatments of photoaging, Photodermatol. Photoimmunol. Photomed. 31 (2) (2015) 65–74.
[38] A.C. Bulua, A. Simon, R. Maddipati, M. Pelletier, H. Park, K.Y. Kim, M.N. Sack, D.L. Kastner, R.M. Siegel, Mitochondrial reactive oxygen species promote production of proinflammatory cytokines and are elevated in TNFR1- associated periodic syndrome (TRAPS), J. Exp. Med. 208 (3) (2011) 519–533.
[39] N.S. Bora, B. Mazumder, S. Mandal, P. Patowary, D. Goyary, P. Chattopadhyay, S.K. Dwivedi, Amelioration of UV radiation-induced photoaging by a combinational sunscreen formulation via aversion of oxidative collagen degradation and promotion of TGF-β/Smad-mediated collagen production, Eur. J. Pharm. Sci. 127 (2019) 261–275.
[40] F. Gendrisch, P.R. Esser, C.M. Schempp, U. Wölfle, Luteolin as a modulator of skin aging and inflammation, Biofactors 47 (2) (2021) 170–180.
[41] Ming-Hsien Lin, Chi-Feng Hung, Hsin-Ching Sung, Shih-Chun Yang, Huang-Ping Yu, Jia-You Fang, The bioactivities of resveratrol and its naturally occurring derivatives on skin, J. Food Drug Anal. 29 (1) (2021) 15–38.
[42] Hye Shin Ahn, Hyun Jae Kim, Na Changseon, Dae Sik Jang, Yu-Kyong Shin, Sun Hee Lee, The protective effect of adenocaulon himalaicum edgew. And its bioactive compound neochlorogenic acid against UVB-induced skin damage in human dermal fibroblasts and epidermal keratinocytes, Plants 10 (8) (2021) 1669.
[43] F. Forouzanfar, H. Hosseinzadeh, M.B. Khorrami, S. Asgharzade, H. Rakhshandeh, Attenuating effect of portulaca oleracea extract on chronic constriction injury induced neuropathic pain in rats: an evidence of anti-oxidative and anti-inflammatory effects, CNS Neurol. Disord.: Drug Targets 18 (4) (2019) 342–349.
[44] Y. Liu, M. Zhang, H. Zhang, X. Qian, L. Luo, Z. He, Anthocyanins inhibit airway inflammation by downregulating the NF-κB pathway via the miR-138-5p/SIRT1 Axis in asthmatic mice, Int. Arch. Allergy Immunol. 183 (5) (2022) 539–551, 2022.
[45] J. Xie, X. Zhang, L. Zhang, Negative regulation of inflammation by SIRT1, Pharmacol. Res. 67 (1) (2013) 60–67.